http://dx.doi.org/10.5012/bkcs.2013.34.12.3559

Synthesis of Alumina-Grafted Manganese Oxide Particles Using Surfactants through Coprecipitation Method and Their Thermal Properties

Boseong Kwon, Jun-Hwan Park, Seong-Cheol Jang, and Seong-Geun Oh*

*Department of Chemical Engineering, Hanyang University, Seoul 133-791, Korea. *E-mail: seongoh@hanyang.ac.kr*
Received July 29, 2013, Accepted September 5, 2013

Alumina particles were grafted onto the surface of manganese oxide particles *via* the coprecipitation process using surfactant and cosurfactant. The phase of Mn/Al salts (Phase I) and the phase of precipitation agent (Phase II) were prepared in aqueous surfactant solution, separately. Phase II was added into Phase I and the reaction was performed to form the precursors of composites through hydrogen bonding between $Mn(OH)_2$ and $Al(OH)_3$ prepared by the reaction of Mn/Al salts with the precipitation agent. The alumina-grafted manganese oxide particles were obtained as a final product after calcination. The concentrations of Al salt and surfactant were varied to investigate their effects on the formation and the crystallinity of composites. In addition, the crystal structure of products could be controlled by changing the calcination temperature. Through thermal analyses, it was found that the thermal stability of manganese oxide was improved by the introduction of alumina on its surface.

Key Words : Manganese oxide, Alumina, Surfactant, Coprecipitation process, Thermal properties

Introduction

Manganese oxide particles have been applied in many industrial fields such as ion sieves, lithium-ion batteries, high density magnetic storage media, magnetic resonance imaging, drug delivery system, and catalysis due to their unique physical and chemical properties.[1-6] Among manganese oxide materials having different Mn oxidation states, Mn_2O_3 is known as an inexpensive and an environment-friendly catalyst for the decomposition of NO[7] and N_2O[8] and the removal of organic pollutants.[9,10] Also, Mn_2O_3 can be used as a precursor for cathode material ($LiMn_2O_4$) in lithium-ion battery systems.[11-13]

Alumina is a significant material in the fields of ceramics and catalysts because it has good thermal, chemical, and mechanical properties.[14,15] Due to these characteristics, alumina has been widely used as a doping or a supporting material in order to improve the properties of other substances. Xu *et al.* found that the electrical conductivity of silicate perovskite was enhanced by substitution of alumina into its phase.[16] Makarov and Trontelj investigated the effect of alumina addition on the current-voltage (I-V) characteristics and microstructure of (Na,Mn)-doped WO_3 ceramics.[17] Deraz prepared alumina-doped Mn/Fe oxide solids and studied their thermal behaviors and phase transformation processes.[18] Amini and co-workers synthesized alumina-polyaniline nanocomposites *via* a template-guided polymerization of aniline using alumina nanosheets and analyzed their conductivity and cyclic voltammetry.[19] Logar *et al.* fabricated alumina-TiO_2 composites through an *in-situ* sol-gel reaction of TiO_2 precursor on the surface of alumina and investigated their photocatalytic activity.[20] Kwon and co-workers studied the improvement in thermal stability of $LiMn_2O_4$ cathode material in a Li-ion battery by utilizing a coating of alumina which inhibited Mn dissolution.[21]

In this research, alumina-grafted Mn_2O_3 particles were synthesized through the coprecipitation method using Mn nitrate and Al nitrate as starting materials and ammonium hydroxide as a precipitation agent. In order to control the formation and the crystallinity of alumina-Mn_2O_3 composite particles, polyoxyethylenesorbitan monolaurate (Tween 20) and *tert*-butanol (*t*-butanol) were used as a nonionic surfactant and a cosurfactant, respectively. In our previous works, we reported that the enhancement in crystallinity of Mn oxide and the thickness-controlled formation of Mn oxide on the surface of silica could be achieved by using a mixture of surfactant and cosurfactant.[22,23] In addition, the crystal structure and the degree of crystallization of composites were controlled by varying the calcination temperature from 500 °C to 800 °C. The characterizations of synthesized alumina-grafted Mn_2O_3 particles were performed by using XRD, FE-SEM, TEM, EDS, and XPS. Moreover, the thermal properties of obtained products were analyzed with TGA and DSC in order to confirm the effect of alumina on the thermal stability of manganese oxide.

Experimental

Materials. As a manganese salt, manganese nitrate hexahydrate was obtained from Junsei Chemical Company. Aluminium nitrate nonahydrate as an aluminium salt was purchased from Yakuri Pure Chemical Company. Polyoxyethylenesorbitan monolaurate (Tween 20) and *tert*-butanol (*t*-butanol), as a nonionic surfactant and a cosurfactant, were obtained from Sigma-Aldrich Chemical Company. As a precipitation agent, ammonium hydroxide (NH_4OH, 25 wt % ammonia solution) was purchased from Wako Pure Chemical Industries. Acetone, used as a washing agent, was obtained

from Duksan Company. All chemical reagents in this study were analytical grade and used without any further purification. The water used in all experiments was double-distilled and deionized from the Milli-Q Plus system (Millipore, France) having 18.2 MΩ·cm electrical resistivity at 25 °C.

Synthesis of Alumina-Grafted Manganese Oxide Particles. For the formation of alumina-grafted manganese oxide (AMO) particles through the coprecipitation method, the phase of Mn/Al salts (Phase I) and the phase of precipitation agent (Phase II) were prepared in water containing surfactant and cosurfactant, separately. The Phase I included manganese nitrate hexahydrate (3000 mM), aluminium nitrate nonahydrate (0, 3, 30, 60, 300, and 600 mM), Tween 20 (0, 50, 100, and 200 mM), and *t*-butanol (0 and 500 mM). The Phase II consisted of ammonium hydroxide (11.59 mL) and the same concentrations of Tween 20 and *t*-butanol added into the Phase I. The volume ratio of Phase I to Phase II was 1:1. After the Phase II was added into the Phase I, the reaction was performed under magnetic stirring at 25 °C for 5 h. The formed precursors of the composites were centrifuged and washed with acetone and water several times. The obtained samples were dried in a vacuum oven at room temperature for 24 h. Then, the powders were calcined in a furnace at 700 °C for 6 h. Also, the calcination temperature was varied (500, 600, and 800 °C) to control the crystal phase of AMO particles. The reason for the heat treatment of composite particles at 500 °C as the lowest calcination temperature in this research is that aluminium hydroxide can be transformed into alumina through calcination at 500 °C.[24-29]

Characterizations. The crystal structure and the crystallinity of the products were analyzed by using X-ray powder diffraction (XRD, Rigaku D/MAX-2500) from 2θ = 10° to 80° with Cu Kα radiation (λ = 1.54056 Å) measured at 40 kV and 100 mA. The morphology and the size of the particles were examined by field emission scanning electron microscopy (FE-SEM, JEOL JSM-6700F and JEOL JSM-6701F). Before the FE-SEM analysis, the obtained powders were coated with platinum by sputtering at 15 mA for 3 min using a coating machine. For the investigation into the shape of the alumina grafted onto the surface of manganese oxide with transmission electron microscopy (TEM, JEOL JEM-2100), a drop of sample dispersion was placed on carbon-coated copper grids and dried in a drying oven at 40 °C for 24 h. The TEM analysis was performed at an acceleration voltage of 130 kV. Energy-dispersive X-ray spectroscopy (EDS), attached to FE-SEM, was used to confirm the chemical composition of AMO composite particles. In order to identify the chemical state of AMO composites, the analysis with X-ray photoelectron spectroscopy (XPS, Theta Probe Base System, Thermo Fisher Scientific Co.) was carried out by using Al Kα radiation as the excitation source. The binding energy of C 1s level (284.5 eV) was used as the internal reference for the data processing of XPS. The thermal analyses, with thermogravimetric analysis (TGA) and differential scanning calorimetry (DSC), were performed by using the instrument (SDT Q600, TA Instruments) in the temperature range from 25 °C to 1200 °C, with a heating rate of 10 °C/min, using pure nitrogen gas at a flow rate of 100 mL/min.

Results and Discussion

Effect of Al Salt Concentration. Since both $Mn(OH)_2$ and $Al(OH)_3$ formed by the reaction between Mn/Al salts and NH_4OH have very low solubility in water, their precipitation occurs in aqueous solution.[15,30-36] During this precipitation process, the precursors of composites were prepared through the hydrogen bonding between $Mn(OH)_2$ and $Al(OH)_3$. Then, alumina-manganese oxide composite particles could be obtained after the calcination of precursor powders. Figure 1 illustrates the XRD patterns of particles synthesized by varying the concentration of Al salt in the reaction medium from 0 to 300 mM. From these results, it was confirmed that Mn oxide and AMO particles, formed through calcination at 700 °C, had the single phase of Mn_2O_3 (JCPDS number: 41-1442). If aluminium was doped into the inside of crystal structure of manganese oxide, the pure phase of manganese oxide could not be achieved and the other peaks including Al-related characteristic peaks should be observed. However, the Al-related XRD peaks were not found. These results confirm the separate formation of $Al(OH)_3$ and $Mn(OH)_2$ and their hydrogen bonding interaction.

In addition, the characteristic peaks of alumina were not observed in any XRD patterns of AMO samples. The first reason for the absence of peaks for alumina is that the smaller amount of Al salt (0-300 mM) was used than that of Mn salt (1500 mM) in the reaction medium. The second reason is the formation of small and finely dispersed alumina particles on the surface of manganese oxide as reported in other studies.[23,37,38] Also, the crystallinity of Mn_2O_3 (XRD

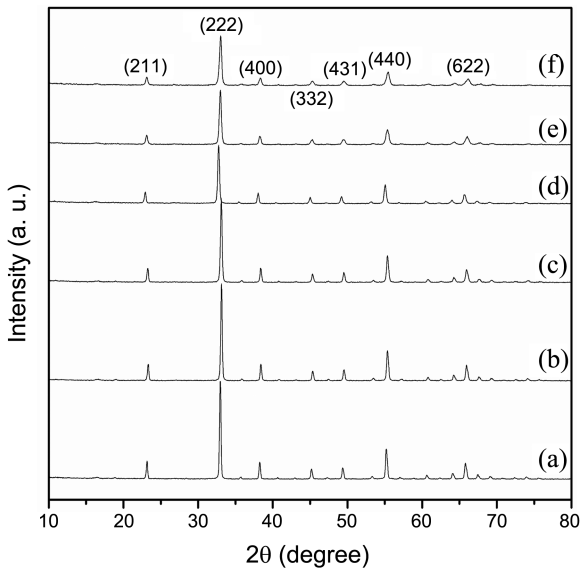

Figure 1. XRD patterns of particles synthesized by using different amount of Al salt: (a) 0 mM, (b) 1.5 mM, (c) 15 mM, (d) 30 mM, (e) 150 mM, and (f) 300 mM (calcination temperature: 700 °C).

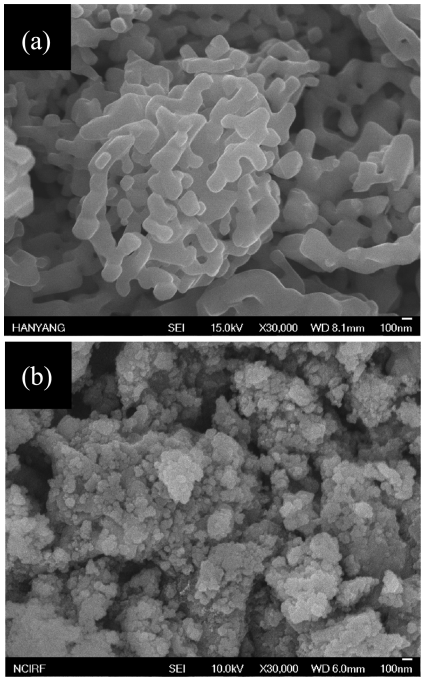

Figure 2. FE-SEM images of (a) Mn_2O_3 and (b) AMO prepared with the addition of 300 mM Al salt (fixed parameter: 700 °C calcination).

intensity of (222) plane) decreased as the amount of aluminium salt increased. This indicates that the crystal growth of Mn_2O_3 was inhibited by grafting the alumina on its surface.

Figure 2(a) and (b) represent the FE-SEM images of Mn_2O_3 and AMO particles prepared without Al salt and with 300 mM of Al salt, respectively. When aluminium nitrate was not used, manganese oxide particles, having a larger and irregularly agglomerated structure, were formed. However, smaller and less aggregated particles were synthesized by adding Al salt 300 mM for the formation of AMO composites. This means that the prevention of crystallization of Mn_2O_3 by alumina occurred with the addition of Al salt. These experimental results are in a good agreement with the previously mentioned XRD data. As illustrated in Figure 3(a), the pristine Mn_2O_3 had a smooth surface. On the other hand, it was confirmed that alumina particles were formed on the surface of manganese oxide through the addition of aluminium nitrate 300 mM (Figure 3(b)). From these experimental results, it was found that the concentration of aluminium salt was a significant factor in controlling the crystallinity and the size of alumina-manganese oxide composite particles.

Influences of Tween 20 and *t*-Butanol. In order to increase the attractive interaction of hydrogen bonding between $Mn(OH)_2$ and $Al(OH)_3$, Tween 20 and *t*-butanol were used as binders. Tween 20 is a nonionic surfactant having three hydroxyl groups in its molecular structure and *t*-butanol is a cosurfactant inducing a dramatic decrease in the surface tension of water with surfactant.[39] Due to these properties, Tween 20 and *t*-butanol in aqueous solution can interact and adsorb onto the surface of hydrophobic Mn and Al hydroxides and then AMO could be more successfully synthesized than AMO prepared without surfactants as shown in Figure 3(b) and (c).[22,23,40] Compared to Figure 3(b), it was shown that the more amount of alumina particles were formed on the surface of smaller Mn_2O_3 particles in Figure 3(c). This indicates that the smaller Mn_2O_3 was synthesized by using surfactant and cosurfactant and then alumina particles were formed on the Mn_2O_3 surface more efficiently. Thus, the alumina particles could be introduced onto the surface of manganese oxide particles more effectively by using surfactant/cosurfactant mixture.

As shown in Figure 4, compared with the XRD intensity of (222) plane of AMO synthesized without Tween 20 and *t*-butanol, the peak intensity decreased by 3.5% and 9.6%, respectively, with an increase of the amount of Tween 20 in the reaction solution (50 mM and 100 mM). When 200 mM of Tween 20 was used, the lowest XRD intensity was observed (decrease by 46.3%). This indicates that more and smaller alumina particles inducing the inhibition of crystal growth of Mn_2O_3 were grafted onto the surface of Mn_2O_3 particles as the amount of Tween 20 was increased. However, characteristic peaks of Mn_3O_4 (JCPDS number: 24-0734) were found in the XRD data of AMO formed by using 100 mM and 200 mM of Tween 20. From these results, it was found that the calcination of samples at 700 °C was not enough for the phase transformation from Mn_3O_4 phase into Mn_2O_3 phase when the AMO particles were prepared by using Tween 20 100 mM and 200 mM with *t*-butanol 500

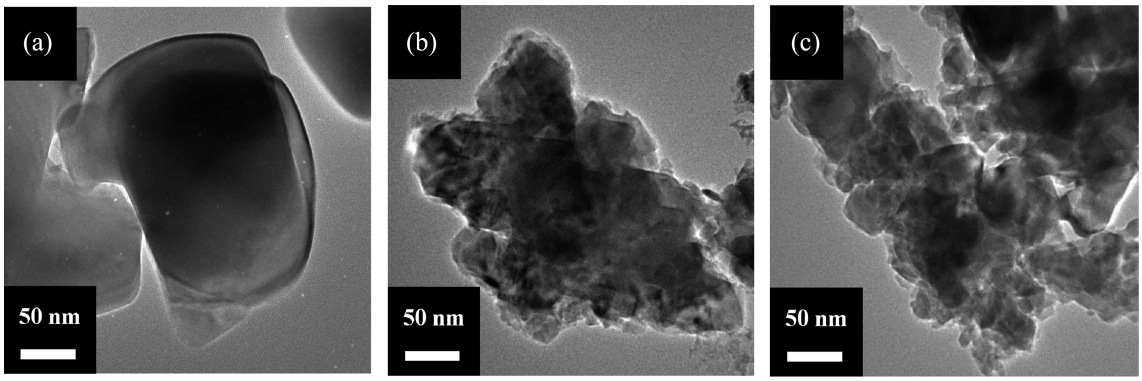

Figure 3. TEM images of products calcined at 700 °C: (a) Mn_2O_3, (b) AMO formed through the addition of 300 mM Al salt, and (c) AMO synthesized by using 300 mM Al salt, 200 mM Tween 20, and 500 mM *t*-butanol.

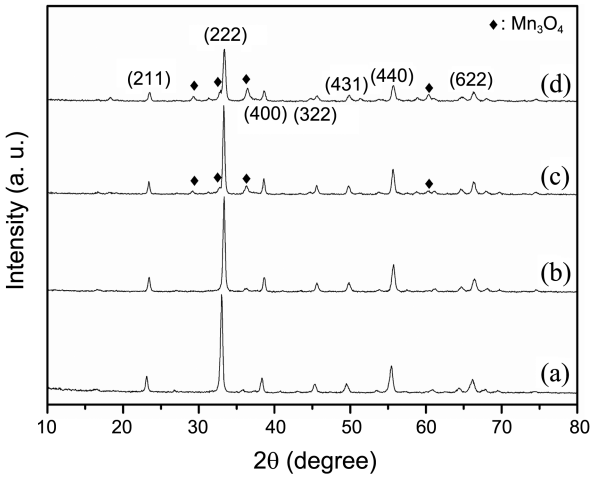

Figure 4. XRD patterns of AMO composite particles obtained by using various concentrations of Tween 20: (a) 0 mM, (b) 50 mM, (c) 100 mM, and (d) 200 mM (fixed parameters: Al salt (300 mM), *t*-butanol (500 mM), and 700 °C calcination). When Tween 20 was not used, *t*-butanol (500 mM) was not added into the reaction medium.

mM. Therefore, the calcination temperature was varied to obtain the pure phase of AMO composites.

Effect of Calcination Temperature. Figure 5 shows the XRD patterns of AMO composite particles synthesized with variations of calcination temperatures from 500 °C to 800 °C at fixed amounts of Al salt (300 mM), Tween 20 (200 mM), and *t*-butanol (500 mM). The crystal structure of manganese oxide materials can be controlled efficiently by changing the temperature of the heat treatment.[41] The single phase of Mn_3O_4 or the mixed phase of Mn_2O_3 and Mn_3O_4 was observed from 500 °C to 700 °C calcination. In this range of calcination temperature, the XRD intensity of Mn_3O_4 phase decreased and the crystallinity of Mn_2O_3 phase increased as the temperature of heat treatment increased. However, the formation of a pure Mn_2O_3 phase could be accomplished

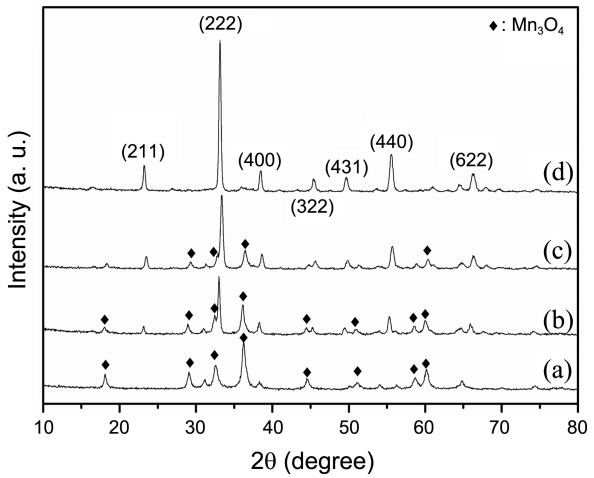

Figure 5. XRD patterns of AMO composites calcined at (a) 500 °C, (b) 600 °C, (c) 700 °C, and (d) 800 °C. The concentrations of Al salt, Tween 20, and *t*-butanol were 300 mM, 200 mM, and 500 mM, respectively.

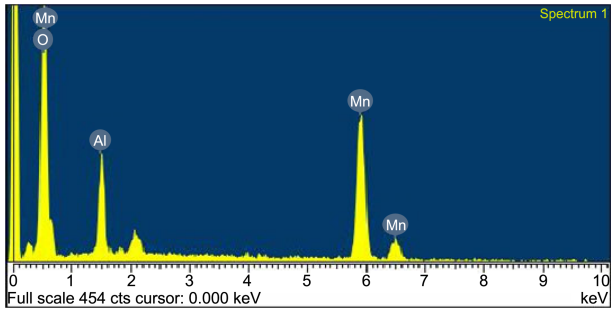

Figure. 6. EDS spectrum of AMO prepared by using Al salt (300 mM), Tween 20 (200 mM), and *t*-butanol (500 mM) (calcination temperature: 800 °C).

through the calcination of AMO composite particles at 800 °C. These results were attributed to the existence of a plentiful amount of Tween 20 and *t*-butanol in the composites. In other words, the higher calcination temperature was needed to remove the entire amount of organic materials. The chemical composition of AMO composite particles prepared by using Al salt (300 mM), Tween 20 (200 mM), and *t*-

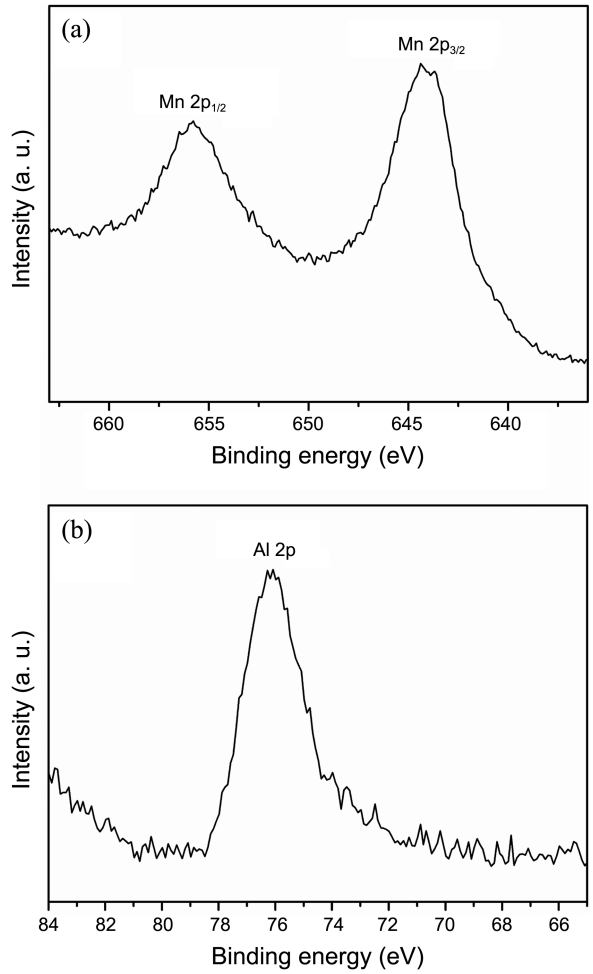

Figure 7. XPS data of AMO composite particles synthesized by using Al salt (300 mM), Tween 20 (200 mM), and *t*-butanol (500 mM) through calcination at 800 °C: (a) Mn 2p spectrum and (b) Al 2p spectrum.

butanol (500 mM) through calcination at 800 °C was investigated by using EDS (Figure 6). Peaks of Mn and Al were observed clearly and the atomic ratio of Mn to Al in the synthesized products was 34.23:9.65. Also, the chemical states of Mn and Al in the composites were analyzed by using XPS as illustrated in Figure 7. As shown in the Mn 2p spectrum, the binding energies of Mn $2p_{1/2}$ and Mn $2p_{3/2}$ were 655.78 eV and 643.89 eV, respectively (Figure 7(a)). These values are higher than those of pristine Mn_2O_3 (653.7 eV and 641.9 eV).[42] This increase in the binding energy of Mn 2p was caused by the interaction between manganese oxide and alumina during the synthetic process.[43] In addition, a higher binding energy of Al 2p (75.83 eV), compared to that in the pure Al_2O_3 (74.60 eV), was observed in the Al 2p spectrum (Figure 7(b)).[44] This shift is attributed to the fine dispersion of alumina on the surface of manganese oxide particles.[45] From these results, it is clear that alumina particles were grafted onto the surface of Mn oxide particles successfully.

Thermal Properties of the Synthesized Products. For the verification of the effect of alumina on the thermal properties of manganese oxide, thermal analyses were used. TGA and DSC thermograms of the pristine Mn_2O_3 and the AMO powders are shown in Figure 8(a) and (b), respectively. From 25 °C to 1200 °C, the weight loss of Mn_2O_3 particles was 5.53 wt % and its endothermic peak was found at approximately 815 °C, which corresponds to the thermal decomposition of Mn_2O_3.[46] On the other hand, in the case of AMO composite particles, 6.2 wt % of weight loss was observed and thermal decomposition appeared around 855 °C. The decreased amount of Mn_2O_3 during the heating of the sample was similar to that of AMO. However, the shift of thermal decomposition temperature was obvious when alumina particles were introduced onto the surface of manganese oxide particles. This indicates that the thermal stability of Mn_2O_3 was enhanced by grafting alumina onto its surface.[47] Thus, the improvement in the thermal stability of Mn_2O_3 could be achieved by the immobilization of finely dispersed alumina particles on the surface of Mn_2O_3 using surfactant and cosurfactant.

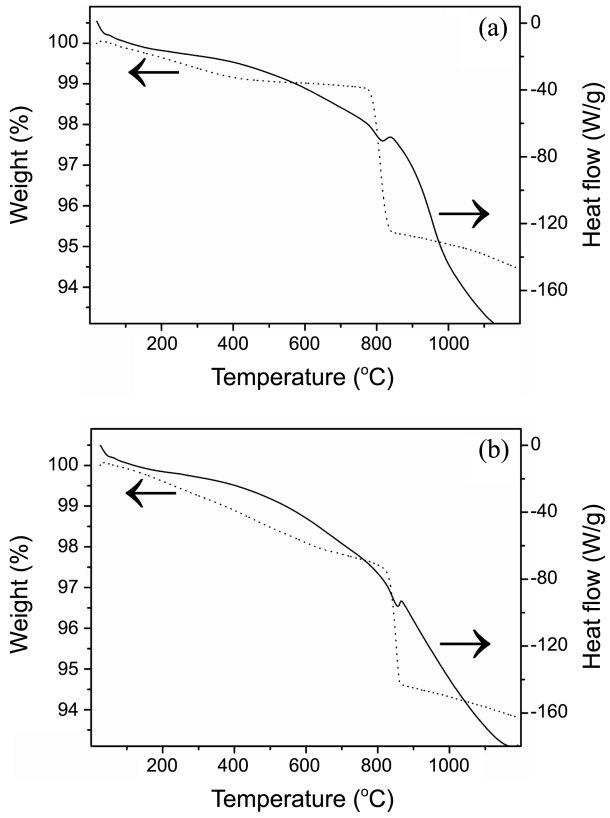

Figure 8. TGA data (dotted line) and DSC data (solid line) of (a) Mn_2O_3 calcined at 700 °C and (b) AMO calcined at 800 °C. The AMO was synthesized with Al salt (300 mM), Tween 20 (200 mM), and *t*-butanol (500 mM).

Conclusion

In summary, alumina-grafted manganese oxide composite particles were synthesized successfully through the coprecipitation process involving hydrogen bonding between $Mn(OH)_2$ and $Al(OH)_3$ and heat treatment at different temperatures. By adding Al salt into the reaction medium, the crystal growth of manganese oxide was inhibited and the formation of alumina on its surface was observed. Also, the introduction of alumina onto the surface of manganese oxide could be controlled effectively by using Tween 20 and *t*-butanol as a surfactant and a cosurfactant. However, a single phase of Mn_3O_4 or a mixed phase of Mn_2O_3 and Mn_3O_4 appeared when large amounts of surfactant and cosurfactant were used. Through the change of calcination temperature, the controls in the crystal phase and the degree of crystallization of products could be achieved. Furthermore, the thermal decomposition temperature of Mn_2O_3 particles was increased from 815 °C to 855 °C when the alumina particles were introduced onto their surface *via* a surfactants-mediated reaction in the coprecipitation process. This result means that the enhancement in the thermal stability of Mn_2O_3 could be accomplished by grafting alumina particles onto the Mn_2O_3 surface using surfactant/cosurfactant mixture. Also, it indicates that the prepared Al_2O_3-grafted Mn_2O_3 with the improved thermal stability can be used as an advanced material in various fields. For example, it is expected that the Mn dissolution from $LiMn_2O_4$ which is a cathode material of lithium rechargeable batteries at high temperature may be decreased by using the Al_2O_3-Mn_2O_3 composite as a precursor of $LiMn_2O_4$. This may result in the enhancement of the electrochemical performance of batteries.

Acknowledgments. This work was supported by the New & Renewable Energy Program of the Korea Institute of Energy Technology Evaluation and Planning (KETEP) grant funded by the Korea government Ministry of Trade, Industry & Energy (No. 20113010010030).

References

1. Aronson, B. J.; Blanford, C. F.; Stein, A. *J. Phys. Chem. B* **2000**, *104*, 449.

2. Ammundsen, B.; Paulsen, J. *Adv. Mater.* **2001**, *13*, 943.
3. Chang, Y. Q.; Xu, X. Y.; Luo, X. H.; Chen, C. P.; Yu, D. P. *J. Cryst. Growth* **2004**, *264*, 232.
4. Gilad, A. A.; Walczak, P.; McMahon, M. T.; Na, H. B.; Lee, J. H.; An, K.; Hyeon, T.; Zijl, P. C. M. V.; Bulte, J. W. M. *Magn. Reson. Med.* **2008**, *60*, 1.
5. Shin, J.; Anisur, R. M.; Ko, M. K.; Im, G. H.; Lee, J. H.; Lee, I. S. *Angew. Chem.-Int. Edit.* **2009**, *48*, 321.
6. Fu, X.; Feng, J.; Wang, H.; Ng, K. M. *Nanotechnology* **2009**, *20*, 375601 (9pp).
7. Yamashita, T.; Vannice, A. *J. Catal.* **1996**, *163*, 158.
8. Imamura, S.; Shono, M.; Okamoto, N.; Hamada, A.; Ishida, S. *Appl. Catal. A-Gen.* **1996**, *142*, 279.
9. Yang, Z.; Zhang, Y.; Zhang, W.; Wang, X.; Qian, Y.; Wen, X.; Yang, S. *J. Solid State Chem.* **2006**, *179*, 679.
10. Cao, J.; Zhu, Y.; Shi, L.; Zhu, L.; Bao, K.; Liu, S.; Qian, Y. *Eur. J. Inorg. Chem.* **2010**, *2010*, 1172.
11. Guo, S.; Zhang, S.; He, X.; Pu, W.; Jiang, C.; Wan, C. *J. Electrochem. Soc.* **2008**, *155*, A760.
12. Guo, H.-J.; Li, X.-H.; Wang, Z.-X.; Peng, W.-J.; Cao, X.; Li, H.-F. *J. Power Sources* **2009**, *189*, 95.
13. Wang, Y.; Shao, X.; Xu, H.; Xie, M.; Deng, S.; Wang, H.; Liu, J.; Yan, H. *J. Power Sources* **2013**, *226*, 140.
14. Uyeda, R. *Prog. Mater. Sci.* **1991**, *35*, 1.
15. Park, J.-Y.; Oh, S.-G.; Paik, U.; Moon, S.-K. *Mater. Lett.* **2002**, *56*, 429.
16. Xu, Y.; McCammon, C.; Poe, B. T. *Science* **1998**, *282*, 922.
17. Makarov, V. O.; Trontelj, M. *J. Eur. Ceram. Soc.* **2000**, *20*, 747.
18. Deraz, N.-A. M. *Thermochim. Acta* **2003**, *401*, 175.
19. Nabid, M. R.; Golbabaee, M.; Moghaddam, A. B.; Mahdavian, A. R.; Amini, M. M. *Polym. Compos.* **2009**, *30*, 841.
20. Logar, M.; Kocjan, A.; Dakskobler, A. *Mater. Res. Bull.* **2012**, *47*, 12.
21. Kim, W.-K.; Han, D.-W.; Ryu, W.-H.; Lim, S.-J.; Kwon, H.-S. *Electrochim. Acta* **2012**, *71*, 17.
22. Park, J.-H.; Kwon, B.; Oh, S.-G. *Chem. Lett.* **2012**, *41*, 1317.
23. Park, J.-H.; Oh, S.-G. *Colloid Surf. A-Physicochem. Eng. Asp.* **2011**, *390*, 199.
24. Sivaraj, Ch.; Reddy, B. P.; Rao, B. R.; Rao, P. K. *Appl. Catal.* **1986**, *24*, 25.
25. Agrafiotis, C.; Tsetsekou, A. *J. Eur. Ceram. Soc.* **2000**, *20*, 815.
26. Chuah, G. K.; Jaenicke, S.; Xu, T. H. *Microporous Mesoporous Mater.* **2000**, *37*, 345.
27. Shaheen, W. M.; Hong, K. S. *Thermochim. Acta* **2002**, *381*, 153.
28. Mercury, J. M. R.; Pena, P.; Aza, A. H. D.; Sheptyakov, D.; Turrillas, X. *J. Am. Ceram. Soc.* **2006**, *89*, 3728.
29. Hollingbery, L. A.; Hull, T. R. *Thermochim. Acta* **2010**, *509*, 1.
30. Jang, Y.-I.; Wang, H.; Chiang, Y.-M. *J. Mater. Chem.* **1998**, *8*, 2761.
31. Anilkumar, M.; Ravi, V. *Mater. Res. Bull.* **2005**, *40*, 605.
32. Gibot, P.; Laffont, L. *J. Solid State Chem.* **2007**, *180*, 695.
33. Liu, D.; Garcia, B. B.; Zhang, Q.; Guo, Q.; Zhang, Y.; Sepehri, S.; Cao, G. *Adv. Funct. Mater.* **2009**, *19*, 1015.
34. Varma, H. K.; Warrier, K. G. K.; Damodaran, A. D. *Ceram. Int.* **1990**, *16*, 73.
35. Li, J.-G.; Ikegami, T.; Lee, J.-H.; Mori, T.; Yajima, Y. *J. Eur. Ceram. Soc.* **2000**, *20*, 2395.
36. Gregory, J.; Duan, J. *Pure Appl. Chem.* **2001**, *73*, 2017.
37. Yu, J. C.; Li, G.; Wang, X.; Hu, X.; Leung, C. W.; Zhang, Z. *Chem. Commun.* **2006**, 2717.
38. Xue, M.; Huang, L.; Wang, J.-Q.; Wang, Y.; Gao, L.; Zhu, J.-H.; Zou, Z.-G. *Nanotechnology* **2008**, *19*, 185604 (8pp).
39. Rosen, M. J. *Surfactants and Interfacial Phenomena*, 3rd ed.; John Wiley & Sons, Inc.: Hoboken, New Jersey, U.S.A., 2004.
40. Esaka, Y.; Kobayashi, M.; Ikeda, T.; Kano, K. *J. Chromatogr. A* **1996**, *736*, 273.
41. Chen, H.; He, J. *J. Phys. Chem. C* **2008**, *112*, 17540.
42. Strohmeier, B. R.; Hercules, D. M. *J. Phys. Chem.* **1984**, *88*, 4922.
43. Kapteijn, F.; Langeveld, A. D. V.; Moulijn, J. A.; Andreini, A.; Vuurman, M. A.; Turek, A. M.; Jehng, J.-M.; Wachs, I. E. *J. Catal.* **1994**, *150*, 94.
44. Chen, M.; Wang, X.; Yu, Y. H.; Pei, Z. L.; Bai, X. D.; Sun, C.; Huang, R. F.; Wen, L. S. *Appl. Surf. Sci.* **2000**, *158*, 134.
45. Wan, H.; Li, D.; Dai, Y.; Hu, Y.; Liu, B.; Dong, L. *J. Mol. Catal. A-Chem.* **2010**, *332*, 32.
46. Xie, X.; Liu, W.; Zhao, L.; Huang, C. *J. Solid State Electrochem.* **2010**, *14*, 1585.
47. Fu, L. J.; Liu, H.; Li, C.; Wu, Y. P.; Rahm, E.; Holze, R.; Wu, H. Q. *Solid State Sci.* **2006**, *8*, 113.